LANGMUIR

Article

pubs.acs.org/Langmuir

Effect of Disjoining Pressure on Surface Nanobubbles

Vitaly B. Svetovoy,[†,‡] Ivan Dević,[†] Jacco H. Snoeijer,[†,§] and Detlef Lohse*[,†,∥]

[†]Physics of Fluids Group, Department of Science and Technology and MESA[+] Institute for Nanotechnology, and JM Burgers Center for Fluid Dynamics, University of Twente, P.O. Box 217, 7500 AE Enschede, The Netherlands

[‡]Institute of Physics and Technology, Yaroslavl Branch, Russian Academy of Sciences, 150007 Yaroslavl, Russia

[§]Department of Applied Physics, Eindhoven University of Technology, P.O. Box 513, 5600 MB Eindhoven, The Netherlands

[∥]Max Planck Institute for Dynamics and Self-Organization, 37077 Göttingen, Germany

ABSTRACT: In gas-oversaturated solutions, stable surface nanobubbles can exist thanks to a balance between the Laplace pressure and the gas overpressure, provided the contact line of the bubble is pinned. In this article, we analyze how the disjoining pressure originating from the van der Waals interactions of the liquid and the gas with the surface affects the properties of the surface nanobubbles. From a functional minimization of the Gibbs free energy in the sharp-interface approximation, we find the bubble shape that takes into account the attracting van der Waals potential and gas compressibility effects. Although the bubble shape slightly deviates from the classical one (defined by the Young contact angle), it preserves a nearly spherical-cap shape. We also find that the disjoining pressure restricts the aspect ratio (size/height) of the bubble and derive the maximal possible aspect ratio, which is expressed via the Young angle.

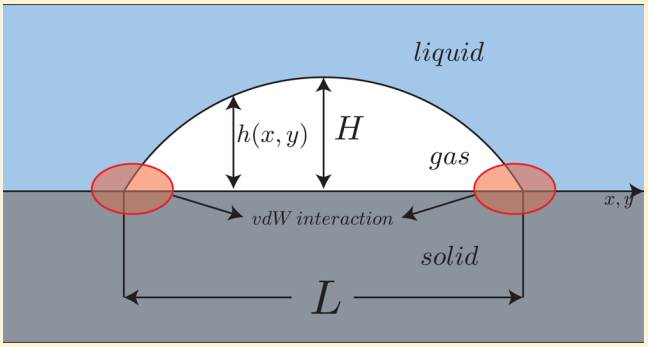

1. INTRODUCTION

When a solid is immersed in liquid under some conditions, nanoscopic spherical-cap-shaped gaseous domains are formed at the interface. These domains, called surface nanobubbles, have attracted a lot of attention recently. (See reviews 1−5.) Their existence and gaseous nature have been confirmed with different methods, but the main challenge was to understand the unexpectedly long lifetime of these bubbles. The surface nanobubbles exist for days instead of microseconds, as expected from the theory of diffusive dissolution.[6] Recently, it was established that contact line pinning of the gas−liquid−solid contact line is crucial to the stability of the bubbles.[7−12] The effect of pinning originates from chemical and topographical heterogeneities of the solid surface,[13−17] which are omnipresent and unavoidable. Given pinning, a stable equilibrium is achieved through the balance of Laplace pressure and gas overpressure due to oversaturation, which is also a necessary condition for stable surface nanobubbles.[11,12] The question we want to address in this article is, how do disjoining pressure effects, a concept introduced to extend the continuum approach down to the nanoscale (e.g., refs 16,18, and 19), modify this balance and the shape of surface nanobubbles?

It is usually assumed that surface nanobubbles can be described by a spherical cap shape. The pressure in such a bubble is constant and equals the ambient pressure plus the Laplace pressure. For liquid drops on a solid, it was already recognized[13,20] that near the contact line the disjoining pressure contributes to the total force balance and influences the equilibrium shape of the drop. The influence of the disjoining pressure on the shape of the drops is, however, rather weak,[21−24] and it is important only at the very edge of the drop. This need not a priori be the case for surface nanobubbles because strong disjoining pressure near the edge could influence the bubble as a whole as a result of the compressibility of the gas. However, this problem has not yet been addressed in detail, though the relevance of the disjoining pressure for nanobubbles and micropancakes has of course been known for a long time.[5,25]

In this article, we will analyze the influence of the van der Waals interaction (i.e., the disjoining pressure) on the equilibrium shape of a free or pinned nanobubble. The article is organized as follows. In Section 2, we briefly review the approach developed for droplets on a solid surface, derive the equation of force balance in the presence of an external field, which is identified with the disjoining pressure, and finally construct the Gibbs free energy for the surface bubble, which can be considered to be a function of the bubble shape. Analytical solutions, which are possible for two-dimensional bubbles, are analyzed in Section 3. Axisymmetric bubbles are discussed in Section 4. Our conclusions are presented and summarized in the last section.

Special Issue: Nanobubbles

Received: May 11, 2016
Revised: May 24, 2016

DOI: 10.1021/acs.langmuir.6b01812
Langmuir XXXX, XXX, XXX−XXX

2. FORMULATION

We aim to establish the shape of surface nanobubbles under the influence of a disjoining pressure. The shape is characterized by the function $h(x, y)$ defined in Figure 1. Here we derive the free-energy functional $\Phi[h]$ using a sharp-interface description from which the equilibrium equations for $h(x, y)$ can be obtained. Assuming an equilibrium implies isothermal conditions; phase transitions that may lead to local cooling are not considered.

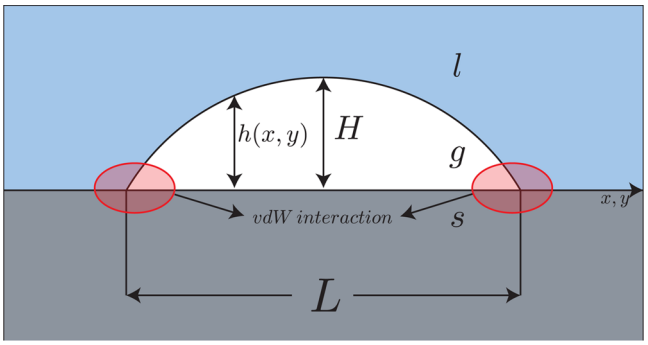

Figure 1. Sketch of a surface nanobubble with vdW interaction (most relevant in the corners) and definitions of the involved parameters. Different media are indicated as liquid (l), gas (g), and solid (s). The local height of the bubble $h(x, y)$ is a function of in-plane coordinates x and y. The maximal height in the center is H, and the footprint size is L.

As a brief reminder, we first summarize the approach commonly used for incompressible liquid drops, which is subsequently extended to incorporate the effect of gas compressibility as is required for surface nanobubbles. We remind the reader that the sketch as expressed in Figure 1 is an approximation. One could also consider a precursor film of the nanobubble toward the surrounding liquid, which would correspond to a local depletion of the water density in direct contact with the wall or similarly to a local gas enhancement because were both found in molecular simulations.[26,27] However, the present sharp-interface description cannot give detailed molecular information, but the fact that such layers are observed in molecular simulations justifies this assumption of our analysis.

2.1. Incompressible Liquid Drops. For incompressible liquid drops, the change in energy when changing the shape can be presented as the functional[17,21−24]

$$\Phi[h] = \int \mathrm{d}x\, \mathrm{d}y \left[\gamma\left(\sqrt{1 + (\nabla h)^2}\right) + \gamma_{sl} - \gamma_{sg} + w(h) + \lambda h\right] \quad (1)$$

Here, γ is the liquid−gas surface tension and the integral gives the surface area. The contribution from a unit area of wetted substrate is $\gamma_{sl} - \gamma_{sg}$, where γ_{sl} and γ_{sg} are the surface tensions for the solid−liquid and solid−gas interfaces, respectively. $w(h)$ represents the van der Waals potential. The Lagrange multiplier λ is introduced to perform the minimization under the constraint of a prescribed finite volume; indeed, integral $\int \mathrm{d}x\, \mathrm{d}y\, h(x, y)$ represents the volume of the droplet.

On the nanoscale, i.e., for nanodrops and nanobubbles, one cannot neglect the range of molecular interactions captured by the effective interface potential $w(h)$. Its influence extends to small h, where the interface is sufficiently close to the substrate. In the variational analysis, which gives the equilibrium equation for $h(x, y)$, the interface potential gives rise to an additional pressure term, $\Pi = -\mathrm{d}w/\mathrm{d}h$, which is the so-called disjoining pressure. In the macroscopic limit, the interface potential simply vanishes, i.e., $w(h = \infty) = 0$. We define the change in the free energy in such a way that it disappears in the "dry" state, which implies that $w(h_c) = \gamma_{sg} - \gamma_{sl} - \gamma$, where h_c is a microscopic cutoff that will be discussed explicitly below. Using Young's law for the macroscopic contact angle θ_Y, this can be written as $-w(h_c) = \gamma(1 - \cos\theta_Y)$. For now, it is of key importance to note that the integral over the disjoining pressure is related to Young's contact angle θ_Y because[21−24,28]

$$-\int_{h_c}^{\infty} \mathrm{d}h\, \Pi(h) = w(\infty) - w(h_c) = \gamma(1 - \cos\theta_Y) \quad (2)$$

Indeed, droplet shapes that minimizes the free energy (eq 1) are very close to a spherical cap, with a macroscopic contact angle θ_Y. The Lagrange multiplier λ represents the Laplace pressure in the drop and can be tuned to achieve the desired drop volume. Only in close proximity to the contact line, where h falls within the range of molecular interactions, does the disjoining pressure alter the droplet shape.

2.2. Pressure Distribution in Compressible Gas Bubbles. Let us now turn our attention to the case of compressible gas bubbles. The obvious first difference with respect to the droplet is that the gas and liquid domains in Figure 1 are inverted. This can be accounted for by exchanging the roles of γ_{sg} and γ_{sl}. However, upon redefining the contact angle in the gas phase (inside the bubble so that $\gamma\cos\theta_Y = \gamma_{sl} - \gamma_{sg}$), both the formalism and the integral relation (eq 2) are still valid. The key difference, however, is the gas compressibility. The energy functional should not be minimized under the constraint of constant volume, but instead we must impose the number of gas molecules N inside the bubble. Namely, surface nanobubbles are observed for a very long time,[1−5] which means that the bubble can be treated as quasi-static and we neglect the escape or influx of molecules due to diffusion. Because of compressibility, a constant number of molecules does not imply a constant volume or a constant pressure inside the bubble.

For simplicity and for specific calculations, we assume that the only source of the disjoining pressure is the van der Waals (vdW) interaction, but this restriction can be easily removed if some other interactions are involved. The interaction becomes strong near the contact line among gas, liquid, and solid (Figure 1). In absence of external fields at the interface separating the liquid and gas phases, temperature T and pressure P stay constant. From the thermodynamic point of view, the vdW interaction can be considered to be an external field acting on the gas molecules located between the opposing walls of the bubble. In a stationary external field, the system becomes inhomogeneous and the pressure along the boundary is not constant anymore. Instead, the chemical potential μ as a function of temperature, pressure, and the parameters characterizing the field stays constant at the interface.[29]

Thermodynamically, μ is the Gibbs free energy per molecule. In an external field, it can be written as

$$\mu = \mu_0(P, T) + \phi(\mathbf{r}) \quad (3)$$

where $\mu_0(P, T)$ is the chemical potential in the absence of the field and $\phi(\mathbf{r})$ is the field potential per molecule, which depends on the position of the molecule $\mathbf{r}$. The bubble will be in mechanical equilibrium if μ = const along the gas−liquid interface. Differentiating eq 3 with respect to the space coordinates, we can find the force balance at the interface

DOI: 10.1021/acs.langmuir.6b01812
Langmuir XXXX, XXX, XXX−XXX

$$\frac{\nabla P}{n(P, T)} + \nabla\phi(\mathbf{r}) = 0 \tag{4}$$

where $n(P, T)$ is the gas concentration in the bubble, and we made use of the thermodynamic relation $(\partial\mu/\partial P)_T = n^{-1}(P, T)$.

As was already mentioned, we assume for definiteness that the opposing walls of the surface nanobubble attract each other with a force per unit area that originates only from the vdW interaction between solid and liquid molecules via the gas gap. This force is

$$\Pi(h) = -\frac{A_H}{6\pi h^3} \tag{5}$$

where $A_H \approx 10^{-20}$ J is the Hamaker constant among liquid, gas, and solid and $h = h(x, y)$ is the local distance between the walls as shown in Figure 1. In the more general case,[28] the vdW interaction is not the only contribution to the disjoining pressure $\Pi(h)$. The local distance h is going to zero in the corners, where the pressure (eq 5) diverges. In reality, this divergence is regularized by hard-core repulsion. Such a regularization is also critical in view of eq 2 because the disjoining pressure in eq 5 cannot be integrated to $h = 0$; this was the reason for introducing a cutoff distance h_c. To control the effect of the cutoff, we explicitly include a repulsive contribution to the disjoining pressure as

$$\Pi(h) = \frac{A_H}{6\pi h^3}\left[\left(\frac{h_c}{h}\right)^6 - 1\right] \tag{6}$$

This pressure is motivated by the body−body Lennard-Jones interaction.[30,31] At $h = h_c$, the repulsive and attractive contributions are equal and the disjoining pressure becomes zero. We note that in eq 6 we have neglected the contribution of spatial partial derivatives to $\Pi(h)$, which in general[19] also depends on $\partial_x h$ and $\partial_{xx} h$, where x represents a spatial coordinate. Given that the contact angle of surface nanobubbles is small, this approximation is justified.

It has to be noted that the pressure (eq 5 or 6) is defined between parallel plates, which is not the case for the bubble walls. We can apply this equation locally by changing the curved surface by flat patches parallel to the substrate. This is the idea of the proximity force approximation[32] (PFA) that is widely used in the analysis of the dispersion forces. (See the recent review in ref 33.) The application of PFA is justified if the radius of curvature of interacting surfaces is much larger than the distance between them. In our case, this condition reads $8H^2/(L^2 + 4H^2) \ll 1$. It will be assumed here that the condition holds true. However, there is no principal problem if the condition is broken. It just means that the specific functional behavior (eq 5 or 6) is changed. Then a more complicated expression has to be used, but one can apply numerical (see the review in ref 34) and sometime analytical[35] methods to determine the $\Pi(h)$ function.

Attraction of the bubble walls results in an extra pressure (disjoining pressure) experienced by a gas molecule. Because of this pressure, the chemical potential at a constant temperature changes on $\Pi(h)v$, where $v = n(P, T)^{-1}$ is the volume per molecule (molar volume). Therefore, the external potential ϕ in eq 3 can be presented as

$$\phi(\mathbf{r}) = \frac{\Pi(h)}{n(P, T)} \tag{7}$$

where both h and P are functions of in-plane coordinates x, y. One can find the functional dependence of pressure by substituting ϕ into the force balance equation (eq 4) and expressing the concentration via the pressure with the help of the equation of state: $n(P, T) = P/kT$. For simplicity, we use here the equation of state for an ideal gas, which can be generalized if necessary. The resulting equation for the coordinate dependence of the pressure is

$$\frac{\nabla P}{P} + \nabla\left(\frac{\Pi(h)}{P}\right) = 0 \tag{8}$$

It can be integrated to find an implicit dependence of P on the local height $h(x, y)$

$$P \ln(P/P_0) = -\Pi(h) \tag{9}$$

where P_0 is the pressure in the bubble if the interaction is switched off ($A_H \to 0$) or when the bubble height reaches macroscopic distances outside the range of molecular interactions. This relation shows explicitly that the pressure in the bubble is not homogeneous. Note that the Hamaker constant for the liquid−gas−solid system is always positive, so the pressure in the bubble is always larger than P_0.

The pressure P as a function of the local height h is shown in Figure 2. It is defined by two independent parameters. One is

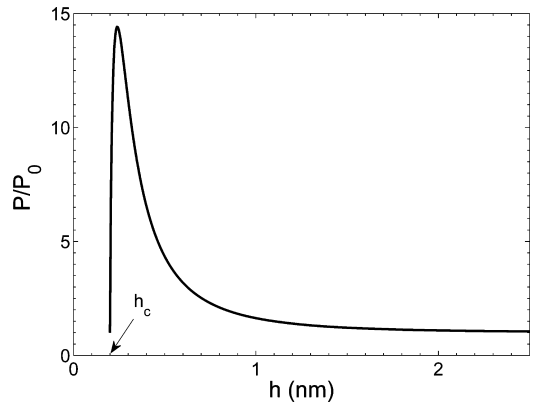

Figure 2. Pressure as a function of the local height for the disjoining pressure (eq 6). The curve is given for parameters $h_c = 0.2$ nm and $A_H/6\pi h_c^3 P_0 = 100$.

the cutoff distance that has typical value of $h_c \approx 0.2$ nm.[36] The second independent parameter is $\beta = A_H/6\pi\, h_c^3 P_0$. At large heights $h \gg h_c$, the pressure asymptotically approaches P_0, has its maximum at $h = 3^{1/6} h_c$, and decreases up to P_0 at $h = h_c$.

2.3. Gibbs Free Energy for Compressible Gas Bubbles.

The thermodynamics of the coexistence of different phases in external fields was considered in ref 37 for a number of physical systems. We construct here the Gibbs free energy $\Phi[h]$ as a function of the bubble shape $h(x, y)$, which consists of volume and surface contributions. The volume contribution is just the sum of the chemical potentials μ for all of the gas molecules inside the bubble:

$$\Phi_V[h] = \int_V \mathrm{d}^3x\, \mu(P, T, h)\, n(P, T) \tag{10}$$

We assume here a sharp interface between liquid and gas (sharp-kink approximation[22]). In this case, the integrand does not depend on the vertical coordinate z, and the corresponding integration can be done explicitly. The lower integration limit z

DOI: 10.1021/acs.langmuir.6b01812
Langmuir XXXX, XXX, XXX−XXX

= 0 corresponds to the solid−gas interface, and the upper limit $z = h$ is at the gas−liquid boundary. Expressing $n(P, T)$ via the equation of state and using the condition μ = const, we find

$$\Phi_V[h] = -\kappa \int dx\, dy\, hP(h) \tag{11}$$

where $\kappa = -\mu/kT$ is an unknown constant, $P(h)$ is the solution of eq 9, and the integral is running over the bubble footprint in the $x - y$ plane. The right-hand side of eq 11 is proportional to the number of molecules in the bubble. The κ constant plays the role of a Lagrange multiplier that imposes the desired number of molecules. Importantly, because pressure $P(h)$ is not constant inside the bubble, this constraint is fundamentally different from the incompressible case, for which the constraint involves the volume $\int dx\, dy\, h$.

The surface contribution to the Gibbs potential $\Phi_S[h]$ can be written as

$$\Phi_S[h] = \int dx\, dy\, [\gamma\sqrt{1 + (\nabla h)^2} + \gamma_{sg} - \gamma_{sl} + w(h)] \tag{12}$$

This is in direct analogy to eq 1 for droplets, except for the interchange between γ_{sg} and γ_{sl} due to the inversion of the liquid and gas phases. The explicit form of the potential in the case of the Lennard-Jones model is

$$w(h) = \frac{A_H}{12\pi h^2}\left[\frac{1}{4}\left(\frac{h_c}{h}\right)^6 - 1\right] \tag{13}$$

Let us stress that the contributions of the interaction to Φ_S and Φ_V are independent. The first one will exist even for a bubble filled with vacuum, while the contribution to Φ_V is related to the gas molecules.

As a result, the total Gibbs free energy can be presented as

$$\begin{aligned}\Phi[h] &= \Phi_V[h] + \Phi_S[h] \\ &= \int dx\, dy\, [\gamma(\sqrt{1 + (\nabla h)^2} - 1) + U(h)]\end{aligned} \tag{14}$$

where using $\gamma(1 - \cos\theta_Y) = -w(h_c)$ we introduced the effective potential

$$U(h) = w(h) - w(h_c) - \kappa h P(h) \tag{15}$$

In combination with eqs 9 and 13, this fully specifies the energy functional for compressible gas bubbles. In the next sections, this functional will be minimized to determine bubble shapes $h(x, y)$.

3. TWO-DIMENSIONAL BUBBLE

We first consider the shape of a two-dimensional (2D) bubble, which is homogeneous in the y direction. In this case, shape $h(x)$ can be obtained analytically and is sufficient to reveal the essential physics. After deriving the general solution, we consider the bubbles with and without pinning. We highlight geometrical features and identify a bound for the aspect ratio for pinned bubbles.

3.1. General Solution. The minimization procedure can be carried out using the Euler−Lagrange method. Namely, for the two-dimensional problem, the functional (eq 14) reduces to the form

$$\Phi[h] = \int dx\, \Gamma(h, h') \tag{16}$$

with the energy per unity length

$$\Gamma(h, h') = \gamma(\sqrt{1 + h'^2} - 1) + U(h) \tag{17}$$

This is the equivalent to a Lagrangian in classical mechanics, in which case the variable is time instead of spatial coordinate x. Minimization of the functional leads to the Euler−Lagrange equations

$$\frac{d}{dx}\frac{\partial\Gamma}{\partial h'} = \frac{\partial\Gamma}{\partial h} \tag{18}$$

and yields the equilibrium equation

$$\gamma\left(\frac{h'}{\sqrt{1 + h'^2}}\right)' = \frac{dU}{dh} = -\Pi(h) - \kappa\frac{d}{dh}[hP(h)] \tag{19}$$

The left-hand side is the Laplace pressure, surface tension times curvature, and the right-hand side contains the disjoining pressure and a term allowing for a finite number of molecules N.

The bubble shape is thus determined by a second-order ordinary differential equation (ODE), which contains κ as an unknown parameter. As boundary conditions, we impose a height H in the center of the bubble, where because of symmetry one also has $h'(0) = 0$:

$$h(0) = H,\ h'(0) = 0 \tag{20}$$

This means that a solution can be generated for each value of κ: by varying κ, one finds bubble shapes that contain a varying number of molecules. We anticipate that a unique equilibrium solution is obtained when it is assumed that there is no pinning of the contact line.

Because in the 2D case the functional does not depend explicitly on x, one can find a first integral of eq 19.[24] It reads

$$\mathcal{E} = h'\frac{\partial\Gamma}{\partial h'} - \Gamma = \gamma\left(1 - \frac{1}{\sqrt{1 + h'^2}}\right) - U(h) \tag{21}$$

where $\mathcal{E}$ is a constant. Again, there is a direct analogy with classical mechanics, where the homogeneity in time enables a first integral of the equation of motion, which expresses the conservation of energy. The analysis is now reduced to eq 21, a first-order ODE with $\mathcal{E}$ and κ as unknown parameters. The value of $\mathcal{E}$ can be eliminated using the boundary conditions (eq 20). This reduces eq 21 to

$$\gamma\left(1 - \frac{1}{\sqrt{1 + h'^2}}\right) = \Delta U(h) \tag{22}$$

where the potential energy difference is introduced

$$\Delta U(h) = U(h) - U(H) \tag{23}$$

An important observation here is that a solution exists only if ΔU is not negative over the entire bubble. In the domain $0 \le x < \infty$, the solution can be presented in an implicit form

$$x = \int_h^H \frac{dh\,(\gamma - \Delta U)}{\sqrt{\Delta U(2\gamma - \Delta U)}} \tag{24}$$

where all of the conditions at $x = 0$ are already satisfied. Note that via eq 15 and $U(h)$, $\Delta U(h)\kappa$ still appears as a parameter, allowing for a family of bubble shapes.

3.2. Homogeneous Substrate: No Pinning. Let us first consider the case where there is no pinning at the contact line, which leads to the true equilibrium solution. For the disjoining

DOI: 10.1021/acs.langmuir.6b01812
Langmuir XXXX, XXX, XXX−XXX

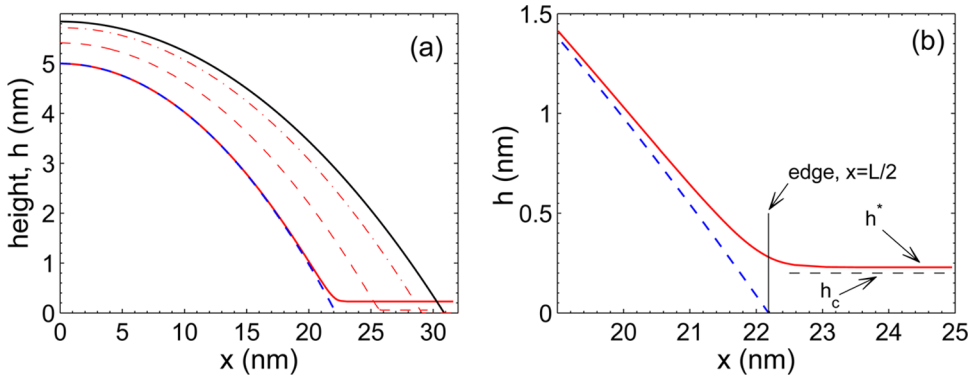

Figure 3. (a) Two-dimensional nanobubble on a homogeneous substrate (solid red curve) with a height of $H = 5$ nm. The dashed blue curve shows the cylindrical cap of an equivalent size L given by eq 25. The black curve presents a classical bubble (i.e., a bubble in the macroscopic description where the influence of the disjoining pressure is replaced by a perfectly localized contact angle boundary condition) containing the same number of molecules. The dashed and dashed−dotted red curves correspond to the reduced interaction with scaling factors (see the text) of $\lambda = 4$ and 256, respectively. (b) Close-up view of the figure near the bubble edge, indicating important parameters as explained in the text.

pressure (eq 6), the balance of attraction and repulsion leads to a solution where the bubble has a precursor film that extends to $x \to \pm\infty$. The film thickness h^* can be determined from the condition $h' = 0$ inside the film. According to eq 22, this implies $\Delta U(h^*) = 0$, and for a given value of H, this selects a unique value of κ and consequently the number of molecules. Note that in the limit of large bubbles $H \to \infty$, much larger than the range of interaction, one has $U(H) \to 0$, which implies that the precursor film thickness $h^* \to h_c$. For small bubbles, the precursor film is a bit larger than h_c.

The existence of the precursor film means that h relaxes to h^* at infinity, and thus the bubble formally extends over the entire domain. Still, we wish to determine a lateral bubble size L. Here we do this by equating the radius of curvature at the top of the bubble to a cylindrical cap, which is the solution for a macroscopic bubble without disjoining pressure. For a cylindrical segment with radius of curvature R, this implies the geometrical connection

$$-\frac{\gamma}{R} = \left.\frac{\mathrm{d}U}{\mathrm{d}h}\right|_{h=H}, \quad R = \frac{(L/2)^2 + H^2}{2H} \tag{25}$$

which effectively defines L.

The shape of a bubble with height $H = 5$ nm is shown in Figure 3 by the solid (red) curve. We took as typical parameters $\gamma = 0.072$ J/m^2, $h_c = 0.2$ nm, and $A_H = 1 \times 10^{-20}$ J. According to eq 2, these parameters correspond to $\theta_Y = 21.4°$. The blue dashed curve is given by eq 25. It defines the cylindrical cap of an equivalent size L. Note that the cap practically coincides with the actual bubble except at the very edge. We found the bubble size and the precursor film thickness to be $L \approx 44.4$ nm and $h^* \approx 0.23$ nm, respectively. The detailed behavior near the edge is shown in Figure 3b, where the bubble edge is marked by the vertical line and the cutoff distance is indicated by the dashed horizontal line. Above the physical edge, the bubble quickly reaches the asymptotic height h^*.

It is interesting to emphasize the effect of the interaction on the bubble size. The bubble that was found by the minimization of the Gibbs free energy (eq 16) can be compared with a classical bubble that has a contact angle θ equal to the Young angle, $\theta = \theta_Y$, and contains the same number of molecules N. These two conditions completely define the classical bubble, which is shown by the black curve in the same figure. It has a lateral size $L^{cl} = 62.2$ nm and a height $H^{cl} = 5.9$ nm. There is a difference between bubbles with and without an interaction potential. This difference is the combined effect of the disjoining pressure and the gas compressibility. How these factors influence the shape and size of the bubble has to be discussed qualitatively.

The pressure in the classical (2D) bubble is estimated to be $P_0^{cl} = P_a + \gamma/R^{cl} \approx 9.46$ bar, where $P_a \approx 1$ bar is the ambient pressure and $R^{cl} \approx 85.1$ nm is the radius of curvature of the classical bubble. The pressure in the bubble with the vdW interaction is distributed inhomogeneously as shown in Figure 2. In the center, it is approaching $P_0 \approx 14.92$ bar and sharply increases near the edges. This inhomogeneous pressure distribution can be responsible only for a small part of the difference between the bubbles. The number of molecules $\mathrm{d}N/\mathrm{d}x \approx h(x)\,P(h)$ in the interval $\mathrm{d}x$ is shown in Figure 4a. For comparison, the same value $\mathrm{d}N/\mathrm{d}x \approx h(x)$ is given for homogeneous pressure $P(h) = P_0$ in the bubble. As one can see, $\mathrm{d}N/\mathrm{d}x$ near the edge is larger than in the case of the

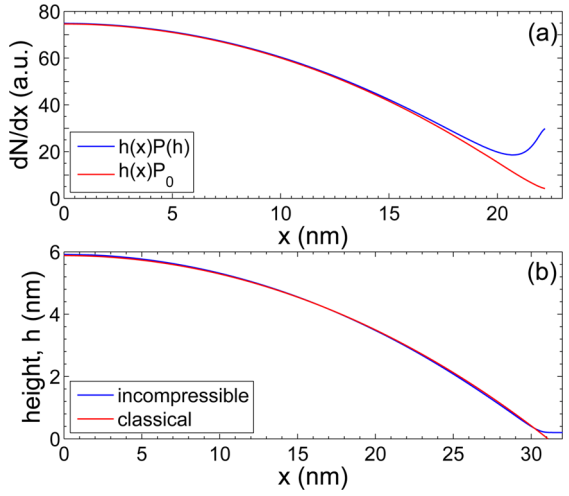

Figure 4. (a) Distribution of the number density $\mathrm{d}N/\mathrm{d}x$ of molecules per length $\mathrm{d}x$ as a function of lateral coordinate x. The blue curve presents the distribution in the actual bubble. The red curve is for an imaginary bubble with homogeneous pressure distribution $P(h(x)) = P_0$. (b) Bubble shape for an incompressible gas in comparison with the classical bubble.

DOI: 10.1021/acs.langmuir.6b01812
Langmuir XXXX, XXX, XXX−XXX

homogeneous pressure, but the integral difference in the number of molecules is just 3%.

In the classical bubble, the vdW interaction is contracted to a line that is the contact line. Without pinning, this line can move freely. If the interaction has a finite distance range, then the contact line moves inward to balance the distributed forces. When the interaction range increases, the classical bubble will shrink more and more. To be sure that this is the case, let us rescale the distance $h \to \lambda h$ in the potential (eq 13), where λ is a scaling factor. This rescaling can be absorbed by the change in the parameters: $A'_H = A_H/\lambda^2$ and $h'_c = h_c/\lambda$. Note that this transformation preserves the basic relation (eq 2). With this transformation, we can change the magnitude of interaction (or equivalently the range of interaction) but keep the same θ_Y. The case $\lambda \to \infty$ corresponds to the classical bubble. In Figure 3, the bubbles for $\lambda = 4$ and 256 are presented by dashed and dashed−dotted curves, respectively. The actual bubble corresponds to $\lambda = 1$. An important observation is that the bubble approaches the classical shape rather slowly when λ increases.

It is also possible to determine what happens if the bubble is filled with an imaginary medium that is an incompressible gas. For that, one has to return to eqs 4 and 7, where we cannot use the equation of state and have to keep the concentration as a constant: $n(P, T) = n_0$. The only change in the Gibbs free energy is the volume term in the effective potential (eq 15), $\kappa h P(h)$, that has to be changed by $\kappa h P_n$, where $P_n = kTn_0$ is a constant with the dimension of pressure. The resulting functional, of course, coincides with that for drops (eq 1). Parameter P_n was chosen to be equal to the pressure in the classical bubble, P_0^{cl}. The condition of a constant number of molecules is equivalent to the condition of constant volume. The result is presented in Figure 4b. One can see that the bubble practically coincides with the classical bubbles except for the behavior near the very edge. Moreover, even the small difference quickly disappears with the increase in scaling factor λ.

We can conclude that the contraction of the bubble in comparison to the classical one in Figure 3 is the result of both the finite interaction range and the gas compressibility.

3.3. Pinned Bubble. If the substrate is not homogeneous, then the bubble size can be determined by the effect of pinning. Pinning of the contact line keeps the lateral extension L as the footprint area of the bubble fixed. This is a crucial assumption for the stability of the surface nanobubbles.[7−12] In this article, we assume that the bottom of the bubble is homogeneous and that inhomogeneities occur at the contact line. This is a reasonable assumption because the interaction is important very close to the bubble edge. Within this approach, we cannot, however, describe the effect of contact angle hysteresis, which is also related to inhomogeneities on the surface.[18,38] To describe the hysteresis, we have to explicitly introduce the dependence of the Hamaker constant on the $x - y$ coordinates.

According to eq 22, the bubble is defined by function $\Delta U(h)$, which via eq 15 depends on parameter κ. This function for three different values of κ is shown in Figure 5. At $h = H$, the function is zero by definition. It has a maximum when the disjoining pressure becomes comparable with the Laplace pressure. At even smaller heights, it also has a minimum when the repulsive interaction becomes comparable with the attraction. Solutions of eq 22 exist only for $\Delta U(h) \geq 0$. There is a minimal value of κ such that for every $\kappa < \kappa_{min}$, function ΔU becomes negative and solutions cease to exist.

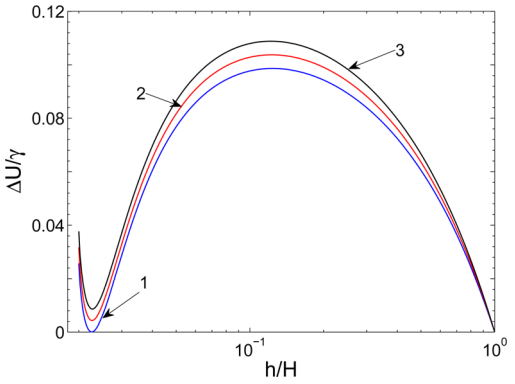

Figure 5. Function $\Delta U(h)$ in units of γ for $H = 5$ nm and $A_H = 1.36 \times 10^{-20}$ J. Curve 1 corresponds to case $\kappa = \kappa_{min}$, which describes the bubble on a homogeneous substrate. Curves 2 and 3 correspond to $\kappa = 1.05\kappa_{min}$ and $1.1\kappa_{min}$, respectively.

This minimal value is defined by the same condition $\Delta U(h^*) = 0$ that we used to determine the unpinned shape. Hence the critical case coincides with the homogeneous unpinned bubble. Expressing κ_{min} from the condition $\Delta U(h^*) = 0$, we find

$$\kappa_{min} = \frac{w(H) - w(h^*)}{HP(H) - h^*P(h^*)} \tag{26}$$

where, as before, h^* is the precursor film thickness. The critical function (curve 1) touches the horizontal axis at one point $h = h^*$. Because the solution (eq 24) is singular in this point, it can be reached only at infinity ($x \to \infty$) so that the domain of heights $h_c < h < h^*$ is not accessible. When $\kappa > \kappa_{min}$, the minimum is positive and all heights $h_c < h < H$ are available. Function $\Delta U(h)$ for $\kappa = 1.05\kappa_{min}$ and $1.10\kappa_{min}$ is presented by curves 2 and 3, respectively.

Three pinned bubbles of the same height, $H = 5$ nm, and different size are shown in Figure 6. Curve 1 shows the bubble,

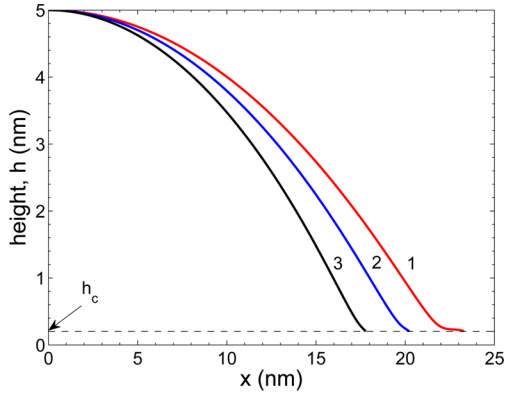

Figure 6. Pinned bubbles at a fixed height $H = 5$ nm and Hamaker constant $A_H = 1 \times 10^{-20}$ J for three different values of $\delta\kappa = \kappa - \kappa_{min}$. Curves 1−3 correspond to $\delta\kappa = 1 \times 10^{-4}$, 0.01, and 0.02, respectively.

which is very close to the critical one. It corresponds to $\delta\kappa = \kappa - \kappa_{min} = 1 \times 10^{-4}$, where $\kappa_{min} = 0.9412$. The size of this bubble, $L = 43.8$ nm, is very close to that of the critical bubble. One can see a distinctive shoulder that remains from the critical bubble but that now has a finite length. Curves 2 and 3 are presented for $\delta\kappa = 0.01$ and 0.02, respectively. The bubble sizes in these cases, $L = 39.8$ and 35.2 nm, are smaller than for the critical bubble, as was expected. It has to be stressed that for pinned

DOI: 10.1021/acs.langmuir.6b01812
Langmuir XXXX, XXX, XXX−XXX

bubbles one cannot demand the continuity of the gas−liquid interface. At the point of pinning, this continuity is broken by the presence of external pinning forces. This is why derivative h' stays constant for the last point of the bubble in contrast to the bubble on the homogeneous substrate.

3.4. Critical Aspect Ratio. With the increase in κ, the bubble size decreases, as one can see from Figure 6 or deduce from eq 25. It means that the bubble with $\kappa = \kappa_{min}$ corresponds to the largest possible bubble for a given height and Hamaker constant. In this sense, we call this bubble a critical bubble. Therefore, the interaction restricts the aspect ratio $\mathcal{R} = L/H$ of the surface nanobubbles: with the increase in $\mathcal{R}$, the surface tension can no longer sustain the increasing interaction. The largest aspect ratio $\mathcal{R}_{cr}$ is realized for the critical bubble. Figure 7 shows $\mathcal{R}_{cr}$ as a function of bubble height H for three different

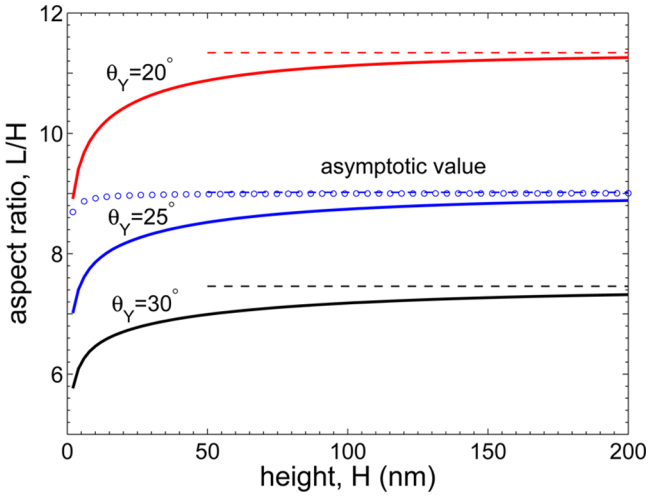

Figure 7. Critical aspect ratio L/H for different Hamaker constants $A_H = 0.87 \times 10^{-20}$, 1.36×10^{-20}, 1.97×10^{-20} J, which are equivalent to Young's angles $\theta_Y = 20, 25, 30°$. The curve shown by open circles was calculated with $\theta_Y = 25°$ for an incompressible gas. The dashed lines give the asymptotic values ($H \to \infty$) for the critical aspect ratios.

values of the Hamaker constant. Actually, instead of A_H we have used in the figure an equivalent parameter θ_Y, which is related to A_H by eq 2. When H becomes large, $\mathcal{R}_{cr}$ saturates at the values shown by the dashed lines. This limit can be found analytically.

As we already mentioned, at $H \to \infty$ the precursor film thickness is reduced to $h^* \to h_c$ and the pressure is reduced to $P(h^*) \to P_0$. Then for κ_{min} in this limit we find from eq 26

$$\kappa_{min} \to -\frac{w(h_c)}{HP_0}, \quad H \to \infty \tag{27}$$

The aspect ratio in the same limit can be determined from eq 25. At the top of a large bubble, the interaction does not contribute, and we find $dU/dh|_{h=H} \to -\kappa P_0$. By substituting into eq 25 together with $\kappa = \kappa_{min}$, we find for the critical aspect ratio

$$\mathcal{R}_{cr} \to 2\sqrt{\frac{1+\cos\theta_Y}{1-\cos\theta_Y}}, \quad H \to \infty \tag{28}$$

where instead of potential $w(h_c)$ we introduce the contact angle according to the relation $\gamma(1 - \cos\theta_Y) = -w(h_c)$. It has to be stressed that this aspect ratio is equivalent to the classical boundary condition: the contact angle is equal to Young's angle, $\theta(L/2) = \theta_Y$, where $\theta(L/2)$ is the contact angle at the bubble's edge.

For small heights, the critical aspect ratio $\mathcal{R}_{cr}$ deviates from the classical limit (eq 28) as Figure 7 demonstrates. For example, even for $H = 200$ nm the deviation from the classical limit is above 2%. Such a strong sensitivity to the interaction was already stressed for bubbles with a fixed number of molecules, and it is related to the compressibility of the gases. We did similar calculations for an incompressible gas, keeping all the other properties of the gas unchanged. The result is strikingly different as demonstrated by the curve shown by the open circles. In this case, 2% deviation is reached only for bubbles with height $H < 5$ nm.

4. AXISYMMETRIC BUBBLE

In the previous section, a significant part of the analysis was carried out analytically, which simplified the understanding of the physical picture. In the case of axisymmetric bubbles, the possibility of an analytical treatment is restricted, but we can use the physical intuition developed in the previous section for the interpretation of the results.

Variation of the total Gibbs free energy (eq 14) results in the equation for the shape of an axisymmetric bubble

$$\frac{\gamma}{r}\left(r\frac{h'}{\sqrt{1+h'^2}}\right)' = \frac{dU}{dh} \tag{29}$$

where $h = h(r)$ is a function of the in-plane radius r and the prime indicates the derivative with respect to r. As in the case of 2D bubbles, the boundary conditions at the top of the bubble are $h(0) = H$ and $h'(0) = 0$. For the axisymmetric bubble, the problem cannot be solved analytically because eq 29 does not have a first integral similar to eq 21.

We expect that on a homogeneous substrate there is a continuous transition at infinity to a precursor film of thickness h^*, $h \to h^*$. Then the boundary condition at $r \to \infty$ is $h' \to 0$. Continuity also demands that the curvature at infinity has to be zero, which is equivalent to the condition $dU/dh \to 0$, and then asymptotically at large r eq 29 is linearized

$$h'' + \frac{h'}{r} = \frac{B}{\gamma}(h - h^*) \tag{30}$$

where B is a constant defined by the effective potential ΔU. The solution of this equation is proportional to the modified Bessel function $K(r\sqrt{B/\gamma})$, which asymptotically at large r has the form

$$h(r) = h^* + \frac{A}{\sqrt{r}}\exp(-r\sqrt{B/\gamma}), \quad r \to \infty \tag{31}$$

where A is an integration constant. The situation here is completely similar to that for the 2D bubble on the homogeneous substrate. The height $h = h^*$ can be reached only at $r \to \infty$. On the other hand, the physical size L is determined by an equation similar to eq 25 with an additional factor of 2 on the left-hand side, which reflects the existence of the two principal curvatures.

The problem was solved numerically using the Runge−Kutta method with the initial conditions $h(0) = H$ and $h'(0) = 0$. Parameter κ was chosen to satisfy the condition $h' \to 0$ at infinity. This bubble describes the critical bubble, which corresponds to the minimal value $\kappa = \kappa_{min}$. Any bubble with

DOI: 10.1021/acs.langmuir.6b01812
Langmuir XXXX, XXX, XXX−XXX

larger κ but with the same height and Hamaker constant is a pinned bubble. Figure 8 shows three bubbles for H = 5 nm and

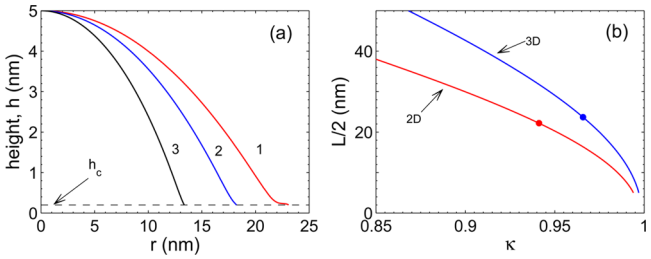

Figure 8. (a) Pinned axisymmetric bubbles for three different values of $\delta\kappa = \kappa - \kappa_{min}$ at fixed H and A_H. Curves 1−3 corresponds to $\delta\kappa = 1 \times 10^{-4}$, 0.01, and 0.02, respectively. (b) Dependence of size L on κ for 2D and 3D cases. The dots correspond to $\kappa = \kappa_{min}$.

$A_H = 1 \times 10^{-20}$ J corresponding to different values of κ. The bubble shown by curve 1 is close to the critical one and corresponds to $\delta\kappa = \kappa - \kappa_{min} = 1 \times 10^{-4}$, where $\kappa_{min} = 0.9658$. Curves 2 and 3 are given for $\delta\kappa = 0.01$ and 0.02, respectively. In comparison to a similar Figure 6 for the 2D case, one can see that the bubble size decreases faster with the increase in κ for purely geometrical reasons. In the inset, the dependence of the bubble size on κ, which follows from eq 25, is shown for both 2D and 3D cases. The minimal κ values are indicated by the dots on each curve. The difference between the 2D and 3D curves originates from different factors in the Laplace pressure (1 vs 2). Close to $\kappa = \kappa_{min}$, derivative $dL/d\kappa$ is larger for the 3D case. This explains the faster variation of L with κ.

The critical aspect ratio as a function of bubble height for axisymmetrical bubbles is shown in Figure 9 for three different

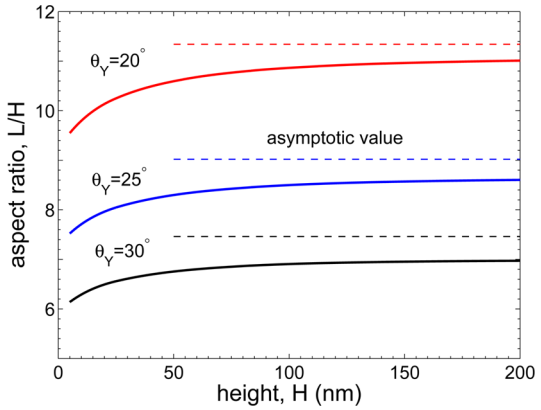

Figure 9. Critical aspect ratio for the axisymmetric bubble as a function of the bubble height. Three presented curves correspond to different Young's angles, θ_Y = 20, 25, and 30° (different Hamaker constants). Thin dashed lines define the classical limit for each Young's angle.

Young's angles (or three different Hamaker constants). Because in the classical limit $H \to \infty$ the same relation (eq 28) for $\mathcal{R}_{cr}$ holds true, the asymptotic limits shown by thin dashed lines are the same as for the 2D case. One can see that the curves behave similarly to those for the 2D case. However, for axisymmetric bubbles the transition to the classical limit happens even more slowly. This is again related to the geometrical reason.

5. CONCLUSIONS

In this article, we considered the influence of the disjoining pressure on the shape, aspect ratio, and pressure distribution inside of the surface nanobubbles. The disjoining pressure was considered to be an external field for the thermodynamic characteristics of the gas filling the bubble. This external field is the reason for the inhomogeneous pressure distribution in the bubble. We characterized the bubble with the Gibbs free energy that includes the standard surface contribution and nontrivial volume contribution. The latter took into account the gas compressibility with a nonuniform pressure distribution. Minimization of the Gibbs free energy allowed for the determination of all of the characteristics of the bubble.

The resulting bubble shape slightly deviates from the classical bubble (defined by Young's contact angle θ_Y) with the same number of molecules but preserves the nearly spherical-cap shape. The deviation is a combined effect of the finite interaction range and the gas compressibility. We found that for a fixed Hamaker constant the bubble aspect ratio L/H (size/height) has to be smaller than a critical value $\mathcal{R}_{cr}(H)$, which depends on the bubble height H. Because of the interaction, a bubble with a small height cannot exist. For large bubbles ($H \to \infty$), the critical aspect ratio approaches that given by the Young's contact angle. We found deviations from this classical limit and established that this effect is related to the gas compressibility. Finally, we stress that the physical idea and the main finding in ref 11, namely, pinning and a stable balance between the Laplace pressure and the gas overpressure as the origin of the stability of surface nanobubbles, remain unaffected by the results in this article.

We did explicit calculations for a van der Waals interaction, although the method applied in this article is much more general. It can be easily generalized to include different contributions that are typically associated with the disjoining pressure. The surface charges on the solid surface or on the gas−liquid interface also could be included.

AUTHOR INFORMATION

Corresponding Author

*E-mail: d.lohse@utwente.nl.

Notes

The authors declare no competing financial interest.

ACKNOWLEDGMENTS

We thank Xuehua Zhang for helpful discussions. This work was supported by The Netherlands Center for Multiscale Catalytic Energy Conversion (MCEC), a NWO Gravitation programme funded by the Ministry of Education, Culture and Science of the government of The Netherlands.

REFERENCES

(1) Hampton, M. A.; Nguyen, A. V. Nanobubbles and the nanobubble bridging capillary force. *Adv. Colloid Interface Sci.* **2010**, *154*, 30−55.

(2) Craig, V. S. J. Very small bubbles at surfaces - the nanobubble puzzle. *Soft Matter* **2011**, *7*, 40−48.

(3) Seddon, J. R. T.; Lohse, D. Nanobubbles and micropancakes: Gaseous domains on immersed substrates. *J. Phys.: Condens. Matter* **2011**, *23*, 133001.

(4) Zhang, X.; Lohse, D. Perspectives on surface nanobubbles. *Biomicrofluidics* **2014**, *8*, 041301.

(5) Lohse, D.; Zhang, X. Surface nanobubble and surface nanodroplets. *Rev. Mod. Phys.* **2015**, *87*, 981−1035.

DOI: 10.1021/acs.langmuir.6b01812
Langmuir XXXX, XXX, XXX−XXX

(6) Epstein, P. S.; Plesset, M. S. On the stability of gas bubbles in liquid-gas solutions. *J. Chem. Phys.* **1950**, *18*, 1505−1509.
(7) Zhang, X.; Chan, D. Y. C.; Wang, D.; Maeda, N. Stability of Interfacial Nanobubbles. *Langmuir* **2013**, *29*, 1017−1023.
(8) Weijs, J. H.; Lohse, D. Why Surface Nanobubbles Live for Hours. *Phys. Rev. Lett.* **2013**, *110*, 054501.
(9) Liu, Y.; Zhang, X. Nanobubble stability induced by contact line pinning. *J. Chem. Phys.* **2013**, *138*, 014706.
(10) Liu, Y.; Wang, J.; Zhang, X.; Wang, W. Contact line pinning and the relationship between nanobubbles and substrates. *J. Chem. Phys.* **2014**, *140*, 054705.
(11) Lohse, D.; Zhang, X. Pinning and gas oversaturation imply stable single surface nanobubble. *Phys. Rev. E* **2015**, *91*, 031003.
(12) Maheshwari, S.; van der Hoef, M.; Zhang, X.; Lohse, D. Stability of Surface Nanobubbles: A Molecular Dynamics Study. *Langmuir* **2016**, DOI: 10.1021/acs.langmuir.6b00963.
(13) de Gennes, P. G. Wetting: statics and dynamics. *Rev. Mod. Phys.* **1985**, *57*, 827−863.
(14) Leger, L.; Joanny, J. F. Liquid spreading. *Rep. Prog. Phys.* **1992**, *55*, 431−486.
(15) Nadkarni, G. D.; Garoff, S. An Investigation of Microscopic Aspects of Contact Angle Hysteresis: Pinning of the Contact Line on a Single Defect. *Europhys. Lett.* **1992**, *20*, 523−528.
(16) Bonn, D.; Eggers, J.; Indekeu, J.; Meunier, J.; Rolley, E. Wetting and spreading. *Rev. Mod. Phys.* **2009**, *81*, 739−805.
(17) Snoeijer, J. H.; Andreotti, B. Moving Contact Lines: Scales, Regimes, and Dynamical Transitions. *Annu. Rev. Fluid Mech.* **2013**, *45*, 269−292.
(18) de Gennes, P. G.; Brochard-Wyart, F.; Quere, D. *Capillarity and Wetting Phenomena: Drops, Bubbles, Pearls, Waves*; Springer: New York, 2004.
(19) Dai, B.; Redondo, A. Disjoining pressure for nonuniform thin films. *Phys. Rev. E* **2008**, *78*, 061602.
(20) Merchant, G. J.; Keller, J. B. Contact angles. *Phys. Fluids A* **1992**, *4*, 477−485.
(21) Dobbs, H.; Indekeu, J. Line tension at wetting: interface displacement model beyond the gradient-squared approximation. *Phys. A* **1993**, *201*, 457−481.
(22) Getta, T.; Dietrich, S. Line tension between fluid phases and a substrate. *Phys. Rev. E: Stat. Phys., Plasmas, Fluids, Relat. Interdiscip. Top.* **1998**, *57*, 655−671.
(23) Schwartz, L. W. Hysteretic Effects in Droplet Motions on Heterogeneous Substrates: Direct Numerical Simulation. *Langmuir* **1998**, *14*, 3440−3453.
(24) Snoeijer, J. H.; Andreotti, B. A microscopic view on contact angle selection. *Phys. Fluids* **2008**, *20*, 057101.
(25) Zhang, X. H.; Maeda, N.; Hu, J. Thermodynamic stability of interfacial gaseous states. *J. Phys. Chem. B* **2008**, *112*, 13671−13675.
(26) Dammer, S. M.; Lohse, D. Gas enrichment at liquid-wall interfaces. *Phys. Rev. Lett.* **2006**, *96*, 206101.
(27) Sendner, C.; Horinek, D.; Bocquet, L.; Netz, R. R. Interfacial water at hydrophobic and hydrophilic surfaces: Slip, viscosity, and diffusion. *Langmuir* **2009**, *25*, 10768−10781.
(28) Churaev, N. V. Contact angles and surface forces. *Adv. Colloid Interface Sci.* **1995**, *58*, 87−118.
(29) Landau, L. D.; Lifshitz, E. M. *Statistical Physics*; Pergamon, 1986; Part 1.
(30) Sellier, M.; Trelluyer, E. Modeling the coalescence of sessile droplets. *Biomicrofluidics* **2009**, *3*, 022412.
(31) Ingebrigtsen, T.; Toxvaerd, S. Contact angles of Lennard-Jones liquids and droplets on planar surfaces. *J. Phys. Chem. C* **2007**, *111*, 8518−8523.
(32) Derjaguin, B. Untersuchungen ueber die Reibung und Adhaesion, IV. *Colloid Polym. Sci.* **1934**, *69*, 155−164.
(33) Svetovoy, V. B.; Palasantzas, G. Influence of surface roughness on dispersion forces. *Adv. Colloid Interface Sci.* **2015**, *216*, 1−19.
(34) Rodriguez, A. W.; Capasso, F.; Johnson, S. G. The Casimir effect in microstructured geometries. *Nat. Photonics* **2011**, *5*, 211−221.
(35) Fosco, C. D.; Lombardo, F. C.; Mazzitelli, F. D. Derivative-expansion approach to the interaction between close surfaces. *Phys. Rev. A: At., Mol., Opt. Phys.* **2014**, *89*, 062120.
(36) Israelachvili, J. *Intermolecular and Surface Forces*; Academic Press, 1991.
(37) Vorob'ev, V. S.; Malyshenko, S. P. Thermodynamics of phase equilibrium in nonuniform fields. *Phys. Rev. E: Stat. Phys., Plasmas, Fluids, Relat. Interdiscip. Top.* **1997**, *56*, 3959−3967.
(38) Joanny, J.; de Gennes, P. A model for contact angle hysteresis. *J. Chem. Phys.* **1984**, *81*, 552.

DOI: 10.1021/acs.langmuir.6b01812
Langmuir XXXX, XXX, XXX−XXX